J. Fluid Mech. (2013), *vol.* 736, *pp.* 67–90.
doi:10.1017/jfm.2013.527

Stability of internal gravity wave beams to three-dimensional modulations

T. Kataoka[1] **and T. R. Akylas**[2,†]

[1]Department of Mechanical Engineering, Graduate School of Engineering, Kobe University, Rokkodai, Nada, Kobe 657-8501, Japan

[2]Department of Mechanical Engineering, Massachusetts Institute of Technology, Cambridge, MA 02139, USA

(Received 23 March 2013; revised 17 July 2013; accepted 27 September 2013; first published online 1 November 2013)

The linear stability of uniform, plane internal wave beams with locally confined spatial profile, in a stratified fluid of constant buoyancy frequency, is discussed. The associated eigenvalue problem is solved asymptotically, assuming perturbations of long wavelength relative to the beam width. In this limit, instability is found only for oblique disturbances which vary in the along-beam and the horizontal transverse directions. The mechanism of instability is a first-harmonic–mean resonant interaction between the underlying wave beam and three-dimensional perturbations that comprise a time-harmonic component, with the beam frequency, and a mean flow. Progressive beams which transport energy in one direction, in particular, are unstable if the beam steepness exceeds a certain threshold value, whereas purely standing beams are unstable even at infinitesimal steepness. A distinguishing feature of this three-dimensional modulational instability is the generation of circulating horizontal mean flows at large distances from the vicinity of the beam.

Key words: geophysical and geological flows, instability, internal waves

1. Introduction

Internal gravity wave beams are fundamental to continuously stratified media and have received considerable attention in the past decade, both from a theoretical perspective and in connection with various geophysical processes. The origin and salient features of wave beams can be readily understood from the well-known dispersion relation obeyed by sinusoidal plane waves in a uniformly stratified Boussinesq fluid; see, for example, Lighthill (1978). A remarkable property of this dispersion relation, reflecting the anisotropic propagation of internal gravity waves, is that the wave frequency depends on the inclination relative to the vertical, but not the magnitude, of the wave vector. By superposition of sinusoidal plane waves with common frequency and wavevectors pointing in the same direction but having different magnitude, therefore, it is possible to construct wave beams: time-harmonic plane waves with general spatial profile that stretch along a direction that depends on the wave frequency. Moreover, as internal waves are transverse, the velocity field associated with such a uniform beam is solely in the beam direction, along which no variations are present. All convective-acceleration terms in the governing equations

† Email address for correspondence: trakylas@mit.edu

of motion thus vanish identically, and a uniform beam, regardless of its profile, represents an exact nonlinear solution in an unbounded, inviscid, uniformly stratified fluid (McEwan 1973; Tabaei & Akylas 2003).

A simple way of generating internal wave beams is by forcing with a localized time-harmonic disturbance at a frequency below the background buoyancy frequency, as demonstrated by Mowbray & Rarity (1967) using an oscillating horizontal cylinder as wave source in a stratified fluid tank. These classic experiments also confirmed that the group velocity is orthogonal to the phase velocity, energy thus being transported along planes of constant phase, an intuitively surprising result which, too, derives from the anisotropy of the internal-wave dispersion relation noted above. Later, Bell (1975) showed analytically that wave beams make up the far-field disturbance induced by a time-harmonic current of stratified fluid of infinite depth over a locally confined bottom obstacle of small amplitude. The suggestion put forward by this simple model for tidal flow over bottom topography in oceans is supported by more recent theoretical and computational investigations (Khatiwala 2003; Lamb 2004) which take into account transient, finite-depth and nonlinear effects ignored in Bell (1975), as well as by laboratory experiments (Gostiaux & Dauxois 2007; Zhang, King & Swinney 2007; Peacock, Echeverri & Balmforth 2008) and field observations (Lien & Gregg 2001; Cole *et al.* 2009; Johnston *et al.* 2011). From these findings, it is now recognized that oceanic internal wave beams are central to tidal conversion – the transfer of tidal energy to internal waves by the interaction of the barotropic tide with sea-floor topography – a process that is believed to be important in deep-ocean mixing. Furthermore, there is evidence from numerical simulations (Fovell, Durran & Holton 1992; Alexander, Holton & Durran 1995) and field experiments (Dewan *et al.* 1998; Kumar 2007) that atmospheric gravity waves due to thunderstorms often form beam-like structures by a mechanism analogous to mechanical forcing (Mowbray & Rarity 1967).

On the theoretical side, since uniform beams are fundamental nonlinear states in an inviscid stratified fluid with constant buoyancy frequency, it is natural to enquire into their stability under departures from these idealized flow conditions. A first attempt to address this issue was made by Tabaei & Akylas (2003), who studied analytically the evolution of slow modulations along a finite-steepness beam with general profile, taking into account weak viscous effects as well as the possible presence of background shear and variations in the buoyancy frequency. Surprisingly enough, nonlinear effects due to along-beam modulations vanish to leading order, and the propagation under the assumed flow conditions is controlled by linear dispersive, viscous and refraction effects; hence, uniform internal wave beams are totally stable to along-beam modulations. While this does not exclude instability to other types of perturbations, the stability characteristics of internal wave beams still remain largely unexplored. An exception is the recent study by Clark & Sutherland (2010), who present experimental and numerical evidence that finite-steepness beams with a quasi-monochromatic profile can be unstable, and eventually break down, due to short-scale plane disturbances with frequency half of that of the underlying beam. This instability mechanism appears to be closely related to the widely studied parametric subharmonic instability of sinusoidal plane internal waves; see Koudella & Staquet (2006) and references given therein.

The present paper, unlike the works cited above, is concerned with three-dimensional perturbations of internal wave beams. Specifically, we examine the stability of uniform beams to oblique modulations which vary slowly in the along-beam and the horizontal transverse directions. Such perturbations would naturally

arise, for example, in tidally generated beams over topography with three-dimensional variations, as is typically the case in the field. The dynamics of oblique modulations turns out to be fundamentally different from that of purely longitudinal modulations considered in Tabaei & Akylas (2003). Owing to the presence of transverse variations, a resonant interaction now becomes possible between the underlying beam and three-dimensional perturbations that comprise a time-harmonic component, with the beam frequency, and a mean flow. This first-harmonic–mean interaction, which can lead to instability of a uniform beam, is analysed by matched asymptotics, and the associated stability eigenvalue problem is solved numerically. Specific results are presented for progressive beams which transport energy in one direction, as is the case for tidally generated beams, as well as purely standing beams which involve no net energy transport. In both cases, instability arises only for oblique perturbations, underscoring the three-dimensional character of the instability mechanism. Progressive beams, however, are found to be unstable only above a threshold steepness – given a locally confined beam profile, its peak velocity amplitude has to exceed a critical value for instability to set in – whereas standing beams turn out to be unstable even at infinitesimal steepness.

According to our results, three-dimensional modulational instability becomes stronger as the beam steepness is increased and/or the beam angle to the horizontal is decreased. The latter trend, in particular, suggests that this instability mechanism should be relevant to tidally generated beams which typically propagate at small angles (in the 3–5° range) to the horizontal. Moreover, our analysis reveals that three-dimensional perturbations are accompanied by circulating horizontal mean flows at large distances from the vicinity of the beam. This unique feature of oblique modulations is akin to the recently observed circulating horizontal mean flow induced by wave beams with both longitudinal and transverse variations (Bordes *et al.* 2012). A large-scale mean horizontal circulation was also noted by King, Zhang & Swinney (2009) in laboratory experiments and numerical simulations of tidal flow over model three-dimensional topography (a half-sphere on a horizontal plane).

2. Stability equations

An inviscid, uniformly stratified Boussinesq fluid supports time-harmonic plane internal gravity waves with general spatial profile. These so-called internal gravity wave beams still obey the familiar internal-wave dispersion relation of sinusoidal plane waves,

$$\omega = N_0 \sin\theta, \tag{2.1}$$

which furnishes the wave frequency ω in terms of the beam angle θ $(0 < \theta < \pi/2)$ to the horizontal, N_0 being the (constant) buoyancy frequency of the medium. For the purpose of discussing the stability of such a uniform beam to three-dimensional perturbations, it is convenient to use a rotated coordinate system, formed by the along-beam (ξ), cross-beam (η) and transverse horizontal (ζ) directions (figure 1). Employing the same scalings as in Tabaei & Akylas (2003) (with the beam width as characteristic length and $1/N_0$ as time scale), the flow-velocity components $\boldsymbol{u} = (u, v, w)$ along (ξ, η, ζ) and the reduced density ρ and pressure p, are then governed by the following dimensionless equations:

$$\boldsymbol{\nabla}\cdot\boldsymbol{u} = 0, \tag{2.2a}$$

$$\rho_t + \boldsymbol{u}\cdot\boldsymbol{\nabla}\rho = -u\sin\theta + v\cos\theta, \tag{2.2b}$$

$$u_t + \boldsymbol{u}\cdot\boldsymbol{\nabla}u = -p_\xi + \rho\sin\theta, \tag{2.2c}$$

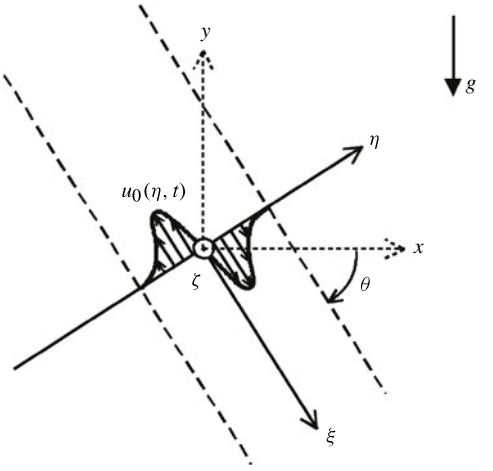

FIGURE 1. Geometry of uniform internal wave beam inclined at an angle θ to the horizontal. The beam profile varies in the cross-beam (η) direction, and the associated flow velocity, $u_0(\eta, t)$, is in the along-beam (ξ) direction. The transverse horizontal direction is denoted by ζ.

$$v_t + \boldsymbol{u} \cdot \nabla v = -p_\eta - \rho \cos\theta, \tag{2.2d}$$

$$w_t + \boldsymbol{u} \cdot \nabla w = -p_\zeta. \tag{2.2e}$$

Equations (2.2) admit the following exact solution representing a finite-steepness internal wave beam (McEwan 1973; Tabaei & Akylas 2003):

$$u = u_0(\eta, t) \equiv \left\{ U(\eta) \mathrm{e}^{-\mathrm{i} \sin\theta t} + \text{c.c.} \right\}, \quad v = w = 0, \tag{2.3a}$$

$$\rho = \rho_0(\eta, t) \equiv \left\{ -\mathrm{i} U(\eta) \mathrm{e}^{-\mathrm{i} \sin\theta t} + \text{c.c.} \right\}, \tag{2.3b}$$

$$p = p_0(\eta, t) \equiv \left\{ \mathrm{i} \cos\theta \int^{\eta} U(\eta') \, \mathrm{d}\eta' \mathrm{e}^{-\mathrm{i} \sin\theta t} + \text{c.c.} \right\}, \tag{2.3c}$$

where c.c. denotes complex conjugate and the amplitude function $U(\eta)$ which specifies the beam profile can be chosen at will. Here, only beams that are locally confined in the cross-beam direction are considered, so $U(\eta) \to 0$ as $\eta \to \pm\infty$. We also assume that the beam angle θ is not equal to the limiting values $\theta = 0$ and $\theta = \pi/2$ for which, respectively, the beam degenerates into a steady horizontal shear flow and a non-propagating fluid column oscillating at the background buoyancy frequency. Moreover, to ensure that the beam (2.3) is statically stable, no density inversions are allowed, which requires that $\partial\rho_0/\partial y < 1$, where $y = \eta \cos\theta - \xi \sin\theta$ denotes the vertical coordinate (figure 1). This condition then translates into

$$\left| \frac{\mathrm{d}U}{\mathrm{d}\eta} \right| < \frac{1}{2\cos\theta}, \tag{2.4}$$

which places a restriction on the maximum steepness of the beam.

We wish to examine the linear stability of the internal wave beam (2.3) to three-dimensional perturbations. To this end, we introduce infinitesimal disturbances to the basic state, in the form of normal modes,

$$u = u_0(\eta, t) + \hat{u}(\eta, t) \exp\{ \mathrm{i}\mu(\xi + c\,t) + \mathrm{i}\varepsilon\zeta \}, \tag{2.5}$$

with analogous expressions for v, w, ρ and p. Here μ and ε are given real wavenumbers, while the mode amplitudes $\hat{\boldsymbol{u}} = (\hat{u}, \hat{v}, \hat{w})$, $\hat{\rho}$ and $\hat{p}$ need to be determined, along with the complex speed c.

Upon substituting (2.5) into (2.2) and linearizing with respect to the perturbations, we find the following set of equations for $\hat{\boldsymbol{u}}$, $\hat{\rho}$ and $\hat{p}$:

$$\mathrm{i}\mu\hat{u} + \frac{\partial\hat{v}}{\partial\eta} + \mathrm{i}\varepsilon\hat{w} = 0, \tag{2.6a}$$

$$\frac{\partial\hat{\rho}}{\partial t} + \sin\theta\,\hat{u} + \left(\frac{\partial\rho_0}{\partial\eta} - \cos\theta\right)\hat{v} = -\mathrm{i}\mu C\hat{\rho}, \tag{2.6b}$$

$$\frac{\partial\hat{u}}{\partial t} - \sin\theta\,\hat{\rho} + \frac{\partial u_0}{\partial\eta}\hat{v} = -\mathrm{i}\mu(C\hat{u} + \hat{p}), \tag{2.6c}$$

$$\frac{\partial\hat{v}}{\partial t} + \cos\theta\,\hat{\rho} + \frac{\partial\hat{p}}{\partial\eta} = -\mathrm{i}\mu C\hat{v}, \tag{2.6d}$$

$$\frac{\partial\hat{w}}{\partial t} + \mathrm{i}\varepsilon\hat{p} = -\mathrm{i}\mu C\hat{w}, \tag{2.6e}$$

where $C = c + u_0$. By the Bloch–Floquet theorem, $\hat{\boldsymbol{u}}$, $\hat{\rho}$ and $\hat{p}$ are to be periodic in t with the same period, $2\pi/\sin\theta$, as the basic state (2.3):

$$(\hat{\boldsymbol{u}}, \hat{\rho}, \hat{p})\big|_{t+2\pi/\sin\theta} = (\hat{\boldsymbol{u}}, \hat{\rho}, \hat{p})\big|_{t}\,. \tag{2.7}$$

In addition, the perturbations must decay in the cross-beam direction, far away from the beam:

$$(\hat{\boldsymbol{u}}, \hat{\rho}, \hat{p}) \to 0 \quad (\eta \to \pm\infty). \tag{2.8}$$

Equations (2.6) along with conditions (2.7) and (2.8) constitute an eigenvalue problem, $c = c_r + \mathrm{i}c_i$ being the eigenvalue parameter. The stability of the underlying wave beam hinges upon the sign of the imaginary part of c, $\mu c_i < 0$ implying instability. In searching for unstable modes, it suffices to consider $\varepsilon > 0$, since a solution of (2.6)–(2.8) for $\varepsilon < 0$ is obtained from that for $\varepsilon > 0$ by $\hat{w} \to -\hat{w}$.

In view of the periodicity requirement (2.7), $\hat{\boldsymbol{u}}$ may be expressed as a Fourier series in t with period $2\pi/\sin\theta$:

$$\hat{\boldsymbol{u}} = \sum_{n=-\infty}^{\infty} \hat{\boldsymbol{U}}_n(\eta)\mathrm{e}^{-\mathrm{i}n\sin\theta t}, \tag{2.9}$$

with analogous expansions for $\hat{\rho}$ and $\hat{p}$. Upon inserting these series and the beam solution (2.3) into (2.6), collecting terms involving like harmonics leads to an infinite set of coupled differential equations for the Fourier coefficients, to be solved subject to the boundary conditions (2.8). For given μ and ε, in general, one could proceed to tackle this problem numerically, by first truncating the Fourier series to a finite number of modes and then discretizing the resulting finite-dimensional boundary-value problem, to obtain a matrix eigenvalue problem for c. Rather than such a fully numerical approach, here we shall analyse the stability problem (2.6)–(2.8) asymptotically, assuming long-wavelength perturbations (μ, $\varepsilon \ll 1$), representing three-dimensional modulations of the uniform beam (2.3). In this limit, as discussed below, the primary ($n = \pm 1$) and mean ($n = 0$) dominate over the rest of the harmonics in (2.9), and a greatly simplified system of coupled equations is obtained from (2.6). However, enforcing the boundary conditions (2.8) requires careful examination of the

far-field flow behaviour in the cross-beam direction. It will turn out that unstable modulations are accompanied by a horizontal mean flow that extends far away from the underlying wave beam.

3. Long-wavelength perturbations

Putting the boundary conditions (2.8) aside, we now seek an asymptotic solution of the stability equations (2.6) subject to the periodicity requirement (2.7) for $\mu, \varepsilon \ll 1$. To proceed in the analysis, these two wavenumbers are taken to satisfy

$$\mu = \kappa\varepsilon^2 \quad (0 < \varepsilon \ll 1), \tag{3.1}$$

κ being an $O(1)$ parameter. Moreover, the cross-beam and transverse velocity amplitudes $\hat{v}$ and $\hat{w}$ are scaled as follows:

$$\hat{v} \to \mu\tilde{v}, \quad \hat{w} \to \varepsilon\tilde{w}. \tag{3.2}$$

Thus, all terms in the incompressibility equation (2.6*a*) are brought to the same order. Under the assumed balance (3.1), it can be readily verified from the dispersion relation (2.1) that modulations along ξ and ζ of a linear sinusoidal plane wave with $O(1)$ wavenumber in the η direction become equally important. As it turns out, the scalings (3.1) and (3.2) are also appropriate for discussing the modulational instability of a small-steepness beam with locally confined cross-section. For a finite-steepness wave beam, however, it will later become necessary to revise (3.1) so as to capture the most unstable modulations (see § 6).

Returning to the stability equations (2.6), after implementing (3.1) and (3.2), the incompressibility equation (2.6*a*) reads

$$\kappa\left(\mathrm{i}\hat{u} + \frac{\partial\tilde{v}}{\partial\eta}\right) + \mathrm{i}\tilde{w} = 0. \tag{3.3a}$$

We also eliminate $\hat{\rho}$ and $\hat{p}$ by first solving for these variables from (2.6*c*) and (2.6*e*) and then substituting the results in (2.6*b*) and (2.6*d*). Thus, the following two equations are obtained:

$$\begin{aligned}\frac{\partial^2\hat{u}}{\partial t^2} + \sin^2\theta\,\hat{u} = \mu\left\{\frac{\partial}{\partial t}\left(\frac{\partial\tilde{w}}{\partial t} - \mathrm{i}C\hat{u} - \frac{\partial u_0}{\partial\eta}\tilde{v}\right) - \mathrm{i}C\frac{\partial\hat{u}}{\partial t}\right.\\ \left. + \sin\theta\left(\cos\theta - \frac{\partial\rho_0}{\partial\eta}\right)\tilde{v}\right\} + O(\mu^2),\end{aligned} \tag{3.3b}$$

$$\begin{aligned}\frac{\partial}{\partial t}\left(\frac{\partial\tilde{w}}{\partial\eta} - \mathrm{i}\cot\theta\,\hat{u}\right) = \mathrm{i}\mu\left\{\frac{\partial\tilde{v}}{\partial t} + \cot\theta\left(\frac{\partial u_0}{\partial\eta}\tilde{v} + \mathrm{i}C\hat{u} - \frac{\partial\tilde{w}}{\partial t}\right)\right.\\ \left. - \frac{\partial}{\partial\eta}(C\tilde{w})\right\} + O(\mu^2).\end{aligned} \tag{3.3c}$$

In view of the periodicity condition (2.7), $\hat{u}$, $\tilde{v}$ and $\tilde{w}$ may be expanded in Fourier series, as in (2.9). For long-wavelength perturbations (μ, $\varepsilon \ll 1$), moreover, (3.3) reveal that the primary and mean harmonics dominate in these series, and the appropriate expansions for $\hat{u}$, $\tilde{v}$ and $\tilde{w}$ take the form

$$\hat{u} = \left\{\hat{U}_-(\eta)\mathrm{e}^{-\mathrm{i}\sin\theta t} + \hat{U}_+(\eta)\mathrm{e}^{\mathrm{i}\sin\theta t}\right\} + \mu\overline{U}(\eta) + \cdots, \tag{3.4a}$$

$$\tilde{v} = \left\{\hat{V}_-(\eta)\mathrm{e}^{-\mathrm{i}\sin\theta t} + \hat{V}_+(\eta)\mathrm{e}^{\mathrm{i}\sin\theta t}\right\} + \overline{V}(\eta) + \cdots, \tag{3.4b}$$

$$\tilde{w} = \left\{\hat{W}_-(\eta)\mathrm{e}^{-\mathrm{i}\sin\theta t} + \hat{W}_+(\eta)\mathrm{e}^{\mathrm{i}\sin\theta t}\right\} + \overline{W}(\eta) + \cdots. \tag{3.4c}$$

Compared to the notation used earlier in (2.9), here the subscripts $\pm$ denote the primary ($n = \pm 1$) and the overbar the mean ($n = 0$) harmonic terms.

The equations governing the amplitudes of the primary and mean harmonics in (3.4) are obtained by inserting these expansions into (3.3) and collecting the various contributions to each harmonic. Specifically, from the primary-harmonic terms in (3.3*c*) and (3.3*a*), we find

$$\hat{W}_\pm = \mathrm{i}\cot\theta \int^\eta \hat{U}_\pm \,\mathrm{d}\eta' + O(\mu), \tag{3.5}$$

$$\hat{V}_\pm = -\mathrm{i}\left(\frac{\mathrm{d}}{\mathrm{d}\eta} + \frac{\mathrm{i}}{\kappa}\cot\theta\right)\int^\eta \int^{\eta'} \hat{U}_\pm \,\mathrm{d}\eta''\,\mathrm{d}\eta' + O(\varepsilon^2). \tag{3.6}$$

Then, collecting primary-harmonic terms in (3.3*b*) and making use of (3.5) and (3.6) yields

$$c\hat{U}_- + \cos\theta\left(\mathrm{i}\frac{\mathrm{d}}{\mathrm{d}\eta} - \frac{1}{2\kappa}\cot\theta\right)\int^\eta \int^{\eta'} \hat{U}_- \,\mathrm{d}\eta''\,\mathrm{d}\eta' - \mathrm{i}\frac{\mathrm{d}U}{\mathrm{d}\eta}\overline{V} = O(\varepsilon^2, \mu), \tag{3.7a}$$

$$c\hat{U}_+ - \cos\theta\left(\mathrm{i}\frac{\mathrm{d}}{\mathrm{d}\eta} - \frac{1}{2\kappa}\cot\theta\right)\int^\eta \int^{\eta'} \hat{U}_+ \,\mathrm{d}\eta''\,\mathrm{d}\eta' - \mathrm{i}\frac{\mathrm{d}U^*}{\mathrm{d}\eta}\overline{V} = O(\varepsilon^2, \mu), \tag{3.7b}$$

where * denotes complex conjugate.

Turning next to mean terms, from (3.3*c*), after further use of (3.5) and (3.6), it follows that

$$c\frac{\mathrm{d}\overline{W}}{\mathrm{d}\eta} + 2\cot\theta\left\{\frac{\mathrm{d}U^*}{\mathrm{d}\eta}\left(\mathrm{i}\frac{\mathrm{d}}{\mathrm{d}\eta} - \frac{1}{2\kappa}\cot\theta\right)\int^\eta \int^{\eta'} \hat{U}_- \,\mathrm{d}\eta''\,\mathrm{d}\eta' + \frac{\mathrm{d}U}{\mathrm{d}\eta}\left(\mathrm{i}\frac{\mathrm{d}}{\mathrm{d}\eta} - \frac{1}{2\kappa}\cot\theta\right)\int^\eta \int^{\eta'} \hat{U}_+ \,\mathrm{d}\eta''\,\mathrm{d}\eta'\right\} = O(\varepsilon^2, \mu). \tag{3.8}$$

Finally, assembling mean terms in (3.3*a*) and (3.3*b*), respectively, we obtain

$$\frac{\mathrm{d}\overline{V}}{\mathrm{d}\eta} = -\frac{\mathrm{i}}{\kappa}\overline{W} + O(\mu), \tag{3.9}$$

$$\sin\theta\,\overline{U} - \cos\theta\,\overline{V} + U^*\hat{U}_- - U\hat{U}_+ + \frac{\mathrm{d}U^*}{\mathrm{d}\eta}\left(\frac{\mathrm{d}}{\mathrm{d}\eta} + \frac{\mathrm{i}}{\kappa}\cot\theta\right)\int^\eta \int^{\eta'} \hat{U}_- \,\mathrm{d}\eta''\,\mathrm{d}\eta' - \frac{\mathrm{d}U}{\mathrm{d}\eta}\left(\frac{\mathrm{d}}{\mathrm{d}\eta} + \frac{\mathrm{i}}{\kappa}\cot\theta\right)\int^\eta \int^{\eta'} \hat{U}_+ \,\mathrm{d}\eta''\,\mathrm{d}\eta' = O(\varepsilon^2, \mu). \tag{3.10}$$

Equations (3.7)–(3.10) bring out the coupling of the primary-harmonic and mean-harmonic perturbations to the underlying internal wave beam: according to (3.8) and (3.10), the interaction of the primary-harmonic perturbation with the beam induces a mean flow, which in turn feeds back to the primary harmonic via interacting with the beam, as described by (3.7). Whether this primary-harmonic–mean interaction mechanism can extract energy from the basic beam, causing instability, depends upon finding modes which, in addition to solving (3.7)–(3.10), remain locally confined in the cross-beam direction, as demanded by the boundary conditions (2.8). This issue is taken up below.

4. Flow behaviour in the far field

Attention is now focused on meeting the boundary conditions (2.8). To this end, we shall require that

$$\int^{\eta}\int^{\eta'}\hat{U}_-\,\mathrm{d}\eta''\,\mathrm{d}\eta'\to 0,\quad \int^{\eta}\int^{\eta'}\hat{U}_+\,\mathrm{d}\eta''\,\mathrm{d}\eta'\to 0\quad(\eta\to\pm\infty). \tag{4.1}$$

In view of (3.5) and (3.6), these conditions ensure that the primary-harmonic perturbations remain locally confined in the cross-beam direction, in accordance with (2.8).

In regard to the mean-flow perturbations, however, as it turns out (see numerical results in § 5), it is not possible to make all three components, $\overline{U}$, $\overline{V}$ and $\overline{W}$, go to zero as $\eta\to\pm\infty$. Instead, following a matched-asymptotics approach, we shall content ourselves with only the largest of these flow components approaching zero, and the remaining mean flow far away from the beam will be matched to an 'outer' disturbance that satisfies the boundary conditions (2.8). Specifically, from the scalings (3.1) and (3.2) and expansions (3.4), the transverse mean flow, being $O(\varepsilon)$, dominates the $O(\mu)$ cross-beam and along-beam mean-flow components. Hence, expanding $\overline{W}$ as follows,

$$\overline{W}=\overline{W}^{(0)}+\kappa\varepsilon\overline{W}^{(1)}+\cdots, \tag{4.2}$$

we impose the condition

$$\overline{W}^{(0)}\to 0\quad(\eta\to\pm\infty). \tag{4.3}$$

Note that, in view of (3.1) and (3.2), the correction term in (4.2) implies that the remaining transverse mean flow in the far field is $O(\mu)$, which is of comparable magnitude to the other two mean-flow components there. In fact, by substituting (4.2) into (3.9), we find that

$$\overline{V}=\overline{V}\big|_{-\infty}-\frac{\mathrm{i}}{\kappa}\int_{-\infty}^{\eta}\overline{W}^{(0)}\,\mathrm{d}\eta'+O(\varepsilon), \tag{4.4}$$

where $\overline{V}|_{-\infty}$ denotes $\overline{V}(\eta\to-\infty)$, and then $\overline{U}$ can be obtained by combining (4.4) with (3.10).

Expressions (4.2) and (4.4) furnish the mean-flow perturbation in the vicinity of the beam; they may be viewed as an 'inner' solution which is to be matched to an 'outer' solution far away from the beam in the cross-beam direction. In preparation for this matching, it follows from (4.2) and (4.4), along with (3.10) and (3.2), that

$$\hat{\boldsymbol{u}}\sim\mu\left(\cot\theta\overline{V}|_{\pm\infty},\overline{V}|_{\pm\infty},\overline{W}^{(1)}|_{\pm\infty}\right)\quad(\eta\to\pm\infty), \tag{4.5}$$

where

$$\overline{V}|_{+\infty}\sim\overline{V}|_{-\infty}-\frac{\mathrm{i}}{\kappa}\int_{-\infty}^{\infty}\overline{W}^{(0)}\,\mathrm{d}\eta+O(\varepsilon\eta)\quad(\eta\to\infty) \tag{4.6}$$

and $\overline{W}^{(1)}|_{\pm\infty}\equiv\overline{W}^{(1)}(\eta\to\pm\infty)$.

The above outer limit of the inner solution for $\hat{\boldsymbol{u}}$ suggests an outer solution in the form

$$\hat{\boldsymbol{u}}\sim\mu\boldsymbol{\mathcal{U}}(\chi)=\mu(\mathscr{U},\mathscr{V},\mathscr{W}). \tag{4.7}$$

Here, $\chi = \varepsilon\eta$ is a 'stretched' cross-beam coordinate, anticipating a breakdown in expansion (4.6) when $\eta \sim 1/\varepsilon$ in the far field. Upon substituting (4.7) into (2.6), to leading order, the outer solutions consistent with the boundary conditions (2.8) are

$$\mathcal{U} \sim \overline{V}|_{\pm\infty}\left(\cot\theta, 1, \mp\frac{\mathrm{i}}{\sin\theta}\right)\mathrm{e}^{\mp\chi/\sin\theta} \quad (\chi \gtrless 0). \tag{4.8}$$

Hence, matching of the outer solution (4.7)–(4.8) as $\chi \to 0^{\pm}$ with the outer limit of the inner solution (4.5)–(4.6) requires that

$$\overline{W}^{(1)}|_{\pm\infty} \sim \mp\frac{\mathrm{i}}{\sin\theta}\overline{V}|_{\pm\infty} \quad (\eta \to \pm\infty). \tag{4.9}$$

Note that, since $\mathscr{U}/\mathscr{V} = \cot\theta$ in (4.8), the induced mean flow far from the beam is purely horizontal.

The boundary conditions (4.1) and (4.3) combined with the matching conditions (4.9) ensure that the primary-harmonic and mean-flow perturbations are locally confined in the cross-beam direction. These conditions are utilized below, along with (3.7)–(3.9), to formulate an eigenvalue problem for c, which determines the stability of the underlying uniform beam.

5. Preliminary stability results

5.1. *Normalized eigenvalue problem*

Returning to (3.7)–(3.9), it is convenient to work with

$$\psi_{\pm} = \int^{\eta}\int^{\eta'} \hat{U}_{\pm}\,\mathrm{d}\eta''\,\mathrm{d}\eta' \tag{5.1}$$

and the cross-beam mean flow $\overline{V}$ which, according to (3.9), to leading order is given by

$$\frac{\mathrm{d}\overline{V}}{\mathrm{d}\eta} = -\frac{\mathrm{i}}{\kappa}\overline{W}^{(0)}, \tag{5.2}$$

where $\overline{W}^{(0)}$ is the leading-order approximation to the transverse mean flow in (4.2). After the scalings

$$\kappa = \frac{1}{2}\cot\theta\tilde{\kappa}, \quad c = \cos\theta\tilde{c}, \quad U = \frac{1}{2}\cos\theta\tilde{U}, \quad \overline{V} = 2\varphi, \tag{5.3}$$

it follows from (3.7)–(3.9) and the boundary conditions (4.1) and (4.3) that ψ_-, ψ_+ and φ satisfy

$$\tilde{c}\frac{\mathrm{d}^2\psi_-}{\mathrm{d}\eta^2} = -\mathrm{i}\frac{\mathrm{d}\psi_-}{\mathrm{d}\eta} + \frac{\psi_-}{\tilde{\kappa}} + \mathrm{i}\frac{\mathrm{d}\tilde{U}}{\mathrm{d}\eta}\varphi, \tag{5.4a}$$

$$\tilde{c}\frac{\mathrm{d}^2\psi_+}{\mathrm{d}\eta^2} = \mathrm{i}\frac{\mathrm{d}\psi_+}{\mathrm{d}\eta} - \frac{\psi_+}{\tilde{\kappa}} + \mathrm{i}\frac{\mathrm{d}\tilde{U}^*}{\mathrm{d}\eta}\varphi, \tag{5.4b}$$

$$\tilde{c}\frac{\mathrm{d}^2\varphi}{\mathrm{d}\eta^2} = -\frac{1}{\tilde{\kappa}}\left\{\frac{\mathrm{d}\tilde{U}^*}{\mathrm{d}\eta}\left(\frac{\mathrm{d}\psi_-}{\mathrm{d}\eta} + \frac{\mathrm{i}}{\tilde{\kappa}}\psi_-\right) + \frac{\mathrm{d}\tilde{U}}{\mathrm{d}\eta}\left(\frac{\mathrm{d}\psi_+}{\mathrm{d}\eta} + \frac{\mathrm{i}}{\tilde{\kappa}}\psi_+\right)\right\}, \tag{5.4c}$$

with

$$\psi_- \to 0, \quad \psi_+ \to 0, \quad \frac{\mathrm{d}\varphi}{\mathrm{d}\eta} \to 0 \quad (\eta \to \pm\infty). \tag{5.5}$$

Equations (5.4) subject to the boundary conditions (5.5) define an eigenvalue problem for $(\psi_-, \psi_+, \varphi)$, with $\tilde{c}$ being the eigenvalue parameter. Note that, in formulating this problem, the only information needed from the matched-asymptotics analysis of § 4 is condition (4.3), which pertains to the dominant mean-flow component, $\overline{W}^{(0)}$. Later, though, we shall make use of the higher-order matching conditions (4.9) as well, to derive the eigenvalue problems governing the most unstable modulations of finite-steepness beams (see § 6.1) and the stability of beams of very small steepness (see Appendix).

The eigenvalue problem (5.4)–(5.5) was solved numerically employing fourth-order centred finite differences and a standard QZ algorithm for the matrix eigenvalue solver. The discretization was carried out on a non-uniform grid, affording higher resolution in the region of the underlying beam, where eigenmodes exhibit rapid variation. The same numerical procedure was followed for solving the eigenvalue problems derived later in this work (see § 6.2 and the Appendix). The size of the computational domain, $-\eta_\infty \leqslant \eta \leqslant \eta_\infty$, and the number of grid points N that we used varied, depending on the needs of each problem ($\eta_\infty = 30$–200, $N = 100$–500).

In our stability computations, as basic state we used: (i) progressive beams, which transport energy in one direction and are most relevant to internal tides; and (ii) purely standing beams, which involve no net energy transport. Specifically, for $\mathrm{d}\tilde{U}/\mathrm{d}\eta$ which enters in the stability equations (5.4), we chose

$$\frac{\mathrm{d}\tilde{U}(\eta)}{\mathrm{d}\eta} = \begin{cases} U_0 \displaystyle\int_0^\infty A(l)\mathrm{e}^{\mathrm{i}l\eta}\,\mathrm{d}l & \text{(progressive beam)}, \quad (5.6a) \\ \dfrac{1}{2}U_0 \displaystyle\int_{-\infty}^\infty A(l)\mathrm{e}^{\mathrm{i}l\eta}\,\mathrm{d}l = -2U_0\frac{\mathrm{d}}{\mathrm{d}\eta}(\eta\mathrm{e}^{-2\eta^2}) & \text{(standing beam)}, \quad (5.6b) \end{cases}$$

with $A(l) = -l^2\mathrm{e}^{-l^2/8}/\sqrt{8\pi}$, U_0 being a parameter that controls the beam peak amplitude. As explained in Tabaei, Akylas & Lamb (2005), progressive beams comprise plane waves with wavenumbers l of the same sign only, whereas standing beams are made of equal contributions from plane waves with wavenumbers of opposite signs. The specific profiles of $\mathrm{d}(\tilde{U}/U_0)/\mathrm{d}\eta$ in (5.6) are displayed in figure 2.

By virtue of the scalings (5.3), the beam angle θ has dropped out of the normalized eigenvalue problem (5.4)–(5.5). The eigenvalues $\tilde{c}$ thus depend on the beam peak amplitude U_0 and the parameter $\tilde{\kappa}$ which, according to (3.1) and (5.3), controls the relative magnitudes of the along-beam and transverse wavenumbers of the perturbation. Moreover, for the profiles (5.6), whose real and imaginary parts, respectively, are odd and even functions of η, it suffices to consider $\tilde{\kappa} > 0$: a solution for $\tilde{\kappa} < 0$ is obtained from that for $\tilde{\kappa} > 0$ by $\eta \to -\eta$, $\psi_- \to \psi_+$ and $\psi_+ \to \psi_-$. Finally, taking into account (5.3), for the underlying beam to be statically stable, (2.4) requires that

$$U_0 < \frac{1}{2\cos^2\theta}. \tag{5.7}$$

This condition is met irrespective of the beam angle $0 < \theta < \pi/2$ if $U_0 < 0.5$, and for $\cos^{-1}\left(1/\sqrt{2U_0}\right) < \theta < \pi/2$ when $U_0 > 0.5$.

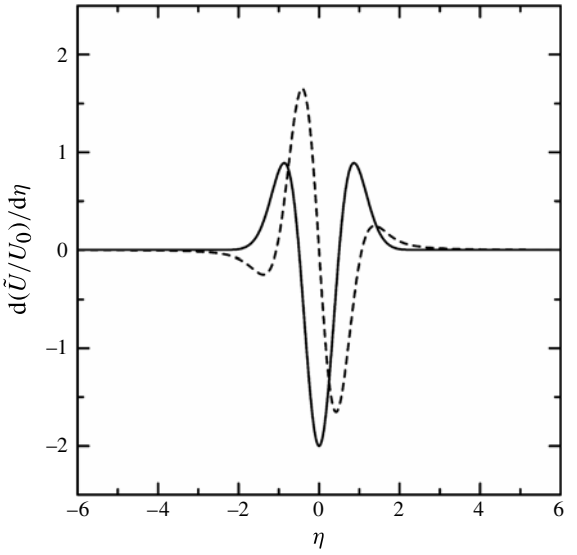

FIGURE 2. Profiles $\mathrm{d}(\tilde{U}/U_0)/\mathrm{d}\eta$ of progressive beam (5.6*a*) (solid line, real part; dashed line, imaginary part) and standing beam (5.6*b*) (solid line).

5.2. *Progressive beams*

Computed eigenvalues $\tilde{c} = \tilde{c}_r + \mathrm{i}\tilde{c}_i$ with negative imaginary part ($\tilde{c}_i < 0$), implying instability, versus $\tilde{\kappa}$ are plotted in figure 3 for the beam amplitudes $U_0 = 0.35$, 0.5 and 0.65. Only results of the greatest growth rate $-\tilde{\kappa}\tilde{c}_i$, corresponding to the most unstable mode, for given $\tilde{\kappa}\,(=2\kappa\tan\theta)$ are presented. Figure 3(*a*) shows that progressive beams with the profile (5.6*a*) are unstable when $U_0 \geqslant 0.35$, and our numerical results indicate that instability is present for U_0 above a critical value of $\sim$0.3.

It is clear from figure 3(*a*) that unstable eigenvalues arise only for $\tilde{\kappa} \neq 0$, revealing that perturbations must have both longitudinal (ξ) and transverse (ζ) variations in order for instability to be possible. Also, it is worth noting that as $\tilde{\kappa} \to \infty$ for fixed U_0, $\tilde{c}$ approaches a constant, and the corresponding growth rate $-\tilde{\kappa}\tilde{c}_i$ increases linearly. This suggests that a rescaling of the assumed balance $\mu = O(\varepsilon^2)$ in (3.1), between the longitudinal and transverse wavenumbers of the perturbation, would be necessary in order to capture the maximum growth rate of the instability (see § 6).

A representative example of instability eigenmode is displayed in figure 4. As expected, the cross-beam mean flow $\overline{V} = 2\varphi$ is not locally confined in η. Qualitatively, $\overline{V}$ is a linear combination of a constant and a tanh-like function. The constant is connected to the outer solutions (4.8) with $\overline{V}|_{+\infty} = \overline{V}|_{-\infty}$, which describe a single horizontal circulating flow per half transverse wavelength (figure 5*a*). In contrast, the tanh-like function is connected to the outer solutions (4.8) with $\overline{V}|_{+\infty} = -\overline{V}|_{-\infty}$, which exhibit two circulating flows bounded by the beam per half transverse wavelength (figure 5*b*). The mean flow in figure 5(*a*) is qualitatively similar to that induced by a wave beam with both longitudinal and transverse variations, according to the experimental observations of Bordes *et al.* (2012).

5.3. *Standing beams*

Computed eigenvalues $\tilde{c}$ with negative imaginary part versus $\tilde{\kappa}$ are plotted in figure 6 for the beam amplitudes $U_0 = 0.1$, 0.4 and 0.65. Unlike the case of progressive

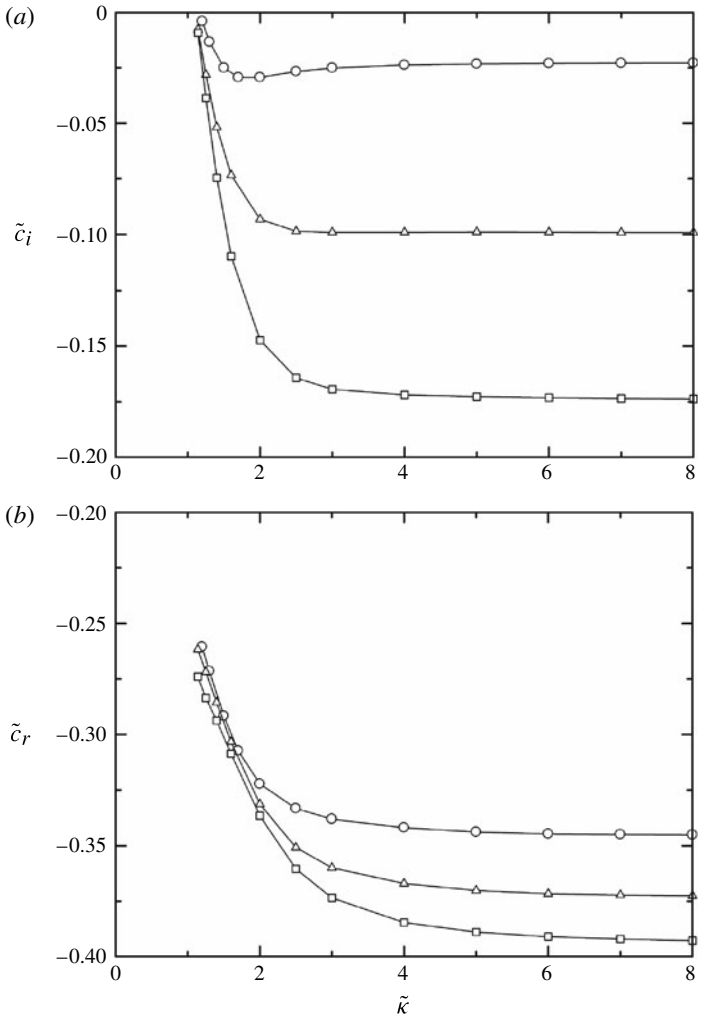

FIGURE 3. Computed eigenvalues $\tilde{c} = \tilde{c}_r + \mathrm{i}\tilde{c}_i$ with negative imaginary part ($\tilde{c}_i < 0$) versus $\tilde{\kappa}$ for progressive beams (5.6*a*): $U_0 = 0.35$ (◯), 0.5 (△) and 0.65 (□); (*a*) $\tilde{c}_i$ versus $\tilde{\kappa}$, (*b*) $\tilde{c}_r$ versus $\tilde{\kappa}$. Only results of the greatest growth rate, $-\tilde{\kappa}\tilde{c}_i$, for given $\tilde{\kappa}$ are presented.

beams where eigenvalues are generally complex, here the most unstable perturbations correspond to pure imaginary $\tilde{c}$, and for $U_0 = 0.4$, 0.65 these eigenvalues first appear at $\tilde{\kappa} = 0$ (figure 6). Also, our computations indicate that standing beams are unstable ($\tilde{c}_i$ stays negative) as $U_0 \to 0$, in spite of the fact that no instability is possible for $U_0 = 0$. This suggests that the stability eigenvalue problem (5.4)–(5.5) is not uniformly valid as $U_0 \to 0$ with $\varepsilon, \mu \ll 1$.

To derive the eigenvalue problem governing the stability of small-steepness beams, a rescaling of (3.7)–(3.9) is necessary. Details of the analysis are given in the Appendix. The proper scaling of the beam profile $U(\eta)$ turns out to be $U = \varepsilon^{1/2} U_S$, and the appropriate eigenvalue problem in the small-steepness limit is (A 7)–(A 8). This problem was solved numerically for the normalized standing-beam profile (5.6*b*), where $U_0 = \varepsilon^{1/2} U_{S0}/\sqrt{\sin\theta}$ (see (A 9)). Computed unstable eigenvalues, which again

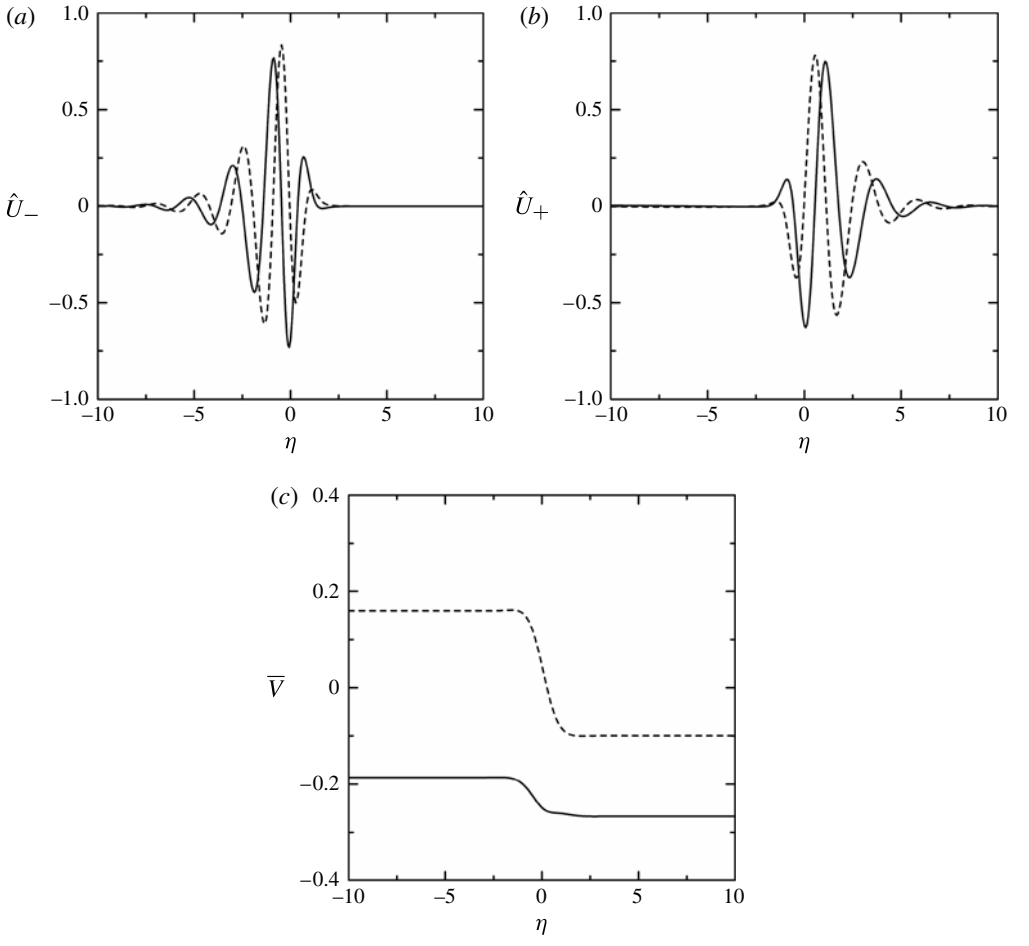

FIGURE 4. Unstable eigenmode versus η for progressive beam (5.6*a*) with $U_0 = 0.5$ and $\tilde{\kappa} = 4$: (*a*) $\hat{U}_-$, (*b*) $\hat{U}_+$, (*c*) $\overline{V}$. The solid line is the real part, and the dashed line is the imaginary part under the normalization $\int_{-\infty}^{\infty} \hat{U}_-(\mathrm{d}\tilde{U}^*/\mathrm{d}\eta)\,\mathrm{d}\eta = 1$.

are pure imaginary, versus $\tilde{\kappa}$ are plotted in figure 7 for various values of the rescaled beam amplitude U_{S0}. It is seen that these eigenvalues as $U_{S0} \to \infty$ agree with those in figure 6 as $U_0 \to 0$. The stability results for small-steepness beams are thus smoothly connected with those for finite-steepness beams. Moreover, as expected, in the limit $U_{S0} \to 0$, no instability is present (specifically the eigenvalues go to zero at U_{S0} around 0.2). Finally, we remark in passing that the eigenvalue problem (A 7)–(A 8) is suitable for examining the stability of small-steepness beams in general. On the basis of this problem, the progressive-beam profile (5.6*a*), in particular, was found to be stable in the small-steepness limit, consistent with the fact that the instability of progressive beams sets in above a certain threshold value of U_0, according to our earlier results (figure 3*a*).

Figures 6 and 7 show that unstable modes ($-\tilde{\kappa}\tilde{c}_i > 0$) arise for $\tilde{\kappa} \neq 0$; hence, perturbations must be three-dimensional for instability to occur, as in the case of progressive beams. Moreover, the eigenvalues $\tilde{c}$ tend to a constant (and the instability growth rate increases linearly) as $\tilde{\kappa} \to \infty$ for finite-steepness beams (figure 6),

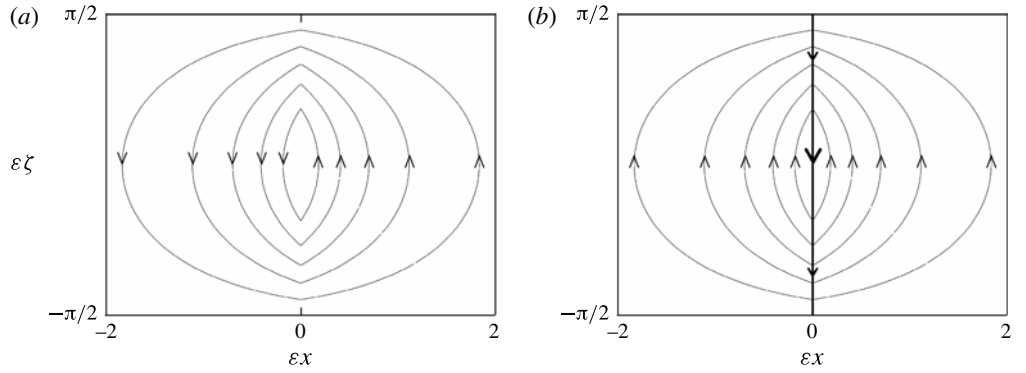

FIGURE 5. Streamline patterns of horizontal mean flows described by the outer solutions (4.8): (*a*) $\overline{V}|_{+\infty} = \overline{V}|_{-\infty}$, (*b*) $\overline{V}|_{+\infty} = -\overline{V}|_{-\infty}$. The thick solid line in (*b*) represents the inner solution which features a strong transverse flow $\overline{W}^{(0)}$ along the beam. The abscissa $\varepsilon x = \varepsilon(\xi\cos\theta + \eta\sin\theta)$ is a horizontal direction perpendicular to the horizontal transverse $\varepsilon\zeta$ direction (figure 1), and streamlines for $|\varepsilon\zeta| > \pi/2$ are symmetric with respect to $\varepsilon\zeta = \pm\pi/2$.

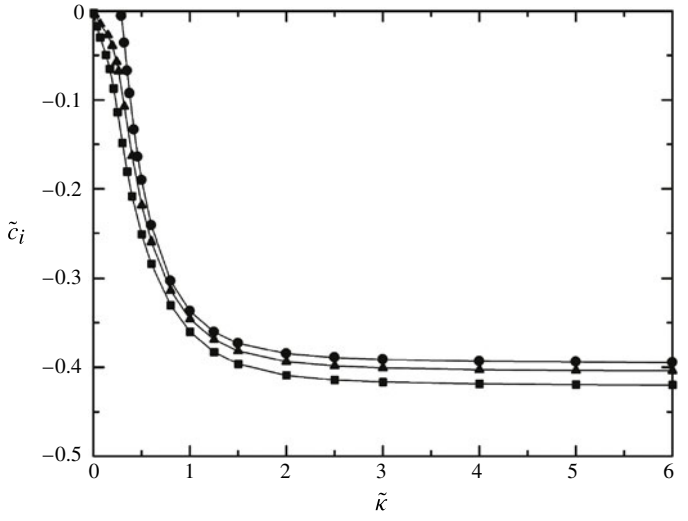

FIGURE 6. Computed unstable eigenvalues $\tilde{c} = \mathrm{i}\tilde{c}_i$ versus $\tilde{\kappa}$ for standing beams (5.6*b*): $U_0 = 0.1$ (●), 0.4 (▲) and 0.65 (■). Only results of the greatest growth rate, $-\tilde{\kappa}\tilde{c}_i$, for given $\tilde{\kappa}$ are presented. (For standing beams with $U_0 \leqslant 0.65$ the most unstable $\tilde{c}$ is pure imaginary.)

whereas for small-steepness beams $\tilde{c}$ eventually falls to zero at a finite value of $\tilde{\kappa}$, which increases as U_{S0} is increased. (In figure 7, for $U_{S0} = 10$ $\tilde{c}$ goes to zero at $\tilde{\kappa} = 16.3$ and for $U_{S0} = 100$ at $\tilde{\kappa} = 163$.) This behaviour suggests that the maximum instability growth rate for finite-steepness standing beams is realized as $\tilde{\kappa} \to \infty$, similar to the case of progressive beams (§ 5.2).

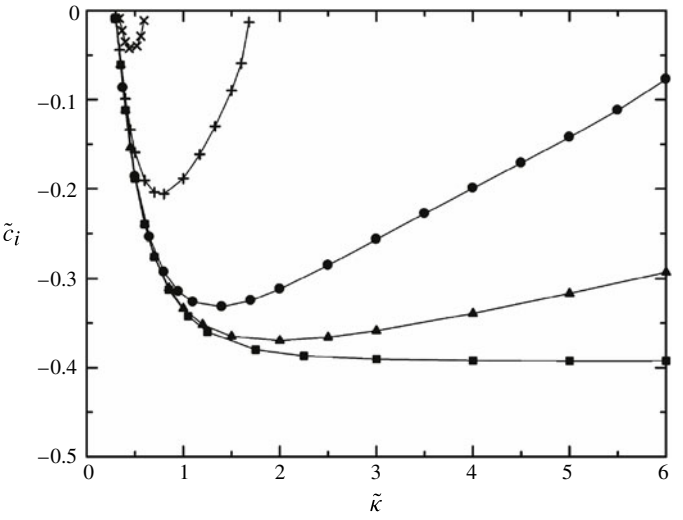

FIGURE 7. Computed unstable eigenvalues $\tilde{c} = \mathrm{i}\tilde{c}_i$ versus $\tilde{\kappa}$ for small-steepness standing beams (5.6*b*) with $U_0 = \varepsilon^{1/2}U_{S0}/\sqrt{\sin\theta}$: $U_{S0} = 0.3$ (×), 1 (+), 4 (●), 10 (▲) and 100 (■). (For small-steepness standing beams there is only one unstable $\tilde{c}$ for given $\tilde{\kappa}$ and it is pure imaginary.)

6. Most unstable modulations

6.1. *Rescaled equations*

For the purpose of capturing the most unstable disturbances of finite-steepness wave beams, we now revise the assumed balance (3.1) between μ and ε, such that $\kappa = \mu/\varepsilon^2 \gg 1$, and rescale (3.7)–(3.9) suitably; this leads to a new eigenvalue problem for c.

Returning to (3.4), when $\kappa \gg 1$, we may expand $\hat{U}_\pm$:

$$\hat{U}_\pm = \hat{U}_\pm^{(0)} + \frac{1}{\kappa}\hat{U}_\pm^{(1)} + \cdots. \tag{6.1}$$

Also, from (3.9),

$$\overline{V} = \overline{V}_\infty - \frac{\mathrm{i}}{\kappa}\int^\eta \overline{W}^{(0)}\,\mathrm{d}\eta' + \cdots, \tag{6.2}$$

where $\overline{V}_\infty$ is a constant, and

$$\overline{W} = \overline{W}^{(0)} + \kappa\varepsilon\overline{W}^{(1)} + \cdots \tag{6.3}$$

according to (4.2). The leading-order term in (6.2) is consistent with the results obtained earlier, for $\kappa \gg 1$, from the eigenvalue problem (5.4)–(5.5): $\overline{V} = 2\varphi$ indeed approaches a constant as $\tilde{\kappa} = 2\kappa\tan\theta \to \infty$, according to (5.4*c*) and (5.5). However, when $\kappa = O(\varepsilon^{-1/2})$, the $O(1/\kappa)$ corrections in (6.1) and (6.2) become as important as the $O(\kappa\varepsilon)$ correction to $\overline{W}$ in (6.3). As a result, in order to capture the dominant instability of finite-steepness wave beams, which is realized as $\kappa \gg 1$, higher-order matching than (4.3) of the inner with the outer mean flow is necessary. To this end, we write

$$\kappa = \frac{\sigma}{\varepsilon^{1/2}}, \tag{6.4}$$

thereby replacing (3.1) with

$$\mu = \sigma \varepsilon^{3/2}, \tag{6.5}$$

where σ is an $O(1)$ parameter.

Upon substituting (6.1)–(6.3), with κ given by (6.4), into (3.7)–(3.8), equating $O(1)$ and $O(\varepsilon^{1/2})$ terms to zero yields

$$c\hat{U}_-^{(0)} = -\mathrm{i}\cos\theta \int^\eta \hat{U}_-^{(0)}\,\mathrm{d}\eta' + \mathrm{i}\frac{\mathrm{d}U}{\mathrm{d}\eta}\overline{V}_\infty, \tag{6.6a}$$

$$c\hat{U}_+^{(0)} = \mathrm{i}\cos\theta \int^\eta \hat{U}_+^{(0)}\,\mathrm{d}\eta' + \mathrm{i}\frac{\mathrm{d}U^*}{\mathrm{d}\eta}\overline{V}_\infty, \tag{6.6b}$$

$$c\frac{\mathrm{d}\overline{W}^{(0)}}{\mathrm{d}\eta} = -2\mathrm{i}\cot\theta\left(\frac{\mathrm{d}U^*}{\mathrm{d}\eta}\int^\eta \hat{U}_-^{(0)}\,\mathrm{d}\eta' + \frac{\mathrm{d}U}{\mathrm{d}\eta}\int^\eta \hat{U}_+^{(0)}\,\mathrm{d}\eta'\right), \tag{6.6c}$$

$$c\hat{U}_-^{(1)} = -\mathrm{i}\cos\theta\int^\eta \hat{U}_-^{(1)}\,\mathrm{d}\eta' + \frac{\cos^2\theta}{2\sin\theta}\int^\eta\int^{\eta'} \hat{U}_-^{(0)}\,\mathrm{d}\eta''\,\mathrm{d}\eta' + \frac{\mathrm{d}U}{\mathrm{d}\eta}\int^\eta \overline{W}^{(0)}\,\mathrm{d}\eta', \tag{6.6d}$$

$$c\hat{U}_+^{(1)} = \mathrm{i}\cos\theta\int^\eta \hat{U}_+^{(1)}\,\mathrm{d}\eta' - \frac{\cos^2\theta}{2\sin\theta}\int^\eta\int^{\eta'} \hat{U}_+^{(0)}\,\mathrm{d}\eta''\,\mathrm{d}\eta' + \frac{\mathrm{d}U^*}{\mathrm{d}\eta}\int^\eta \overline{W}^{(0)}\,\mathrm{d}\eta', \tag{6.6e}$$

$$\begin{aligned} c\frac{\mathrm{d}\overline{W}^{(1)}}{\mathrm{d}\eta} = \frac{2}{\sigma^2}\cot\theta\left\{\frac{\mathrm{d}U^*}{\mathrm{d}\eta}\left(-\mathrm{i}\int^\eta \hat{U}_-^{(1)}\,\mathrm{d}\eta' + \frac{1}{2}\cot\theta\int^\eta\int^{\eta'}\hat{U}_-^{(0)}\,\mathrm{d}\eta''\,\mathrm{d}\eta'\right)\right. \\ \left. + \frac{\mathrm{d}U}{\mathrm{d}\eta}\left(-\mathrm{i}\int^\eta \hat{U}_+^{(1)}\,\mathrm{d}\eta' + \frac{1}{2}\cot\theta\int^\eta\int^{\eta'}\hat{U}_+^{(0)}\,\mathrm{d}\eta''\,\mathrm{d}\eta'\right)\right\}. \end{aligned} \tag{6.6f}$$

In addition, in view of the boundary conditions (4.1) and (4.3) and the matching conditions (4.9), we require that

$$\int^\eta\int^{\eta'}\hat{U}_-^{(0)}\,\mathrm{d}\eta''\,\mathrm{d}\eta' \to 0, \quad \int^\eta\int^{\eta'}\hat{U}_+^{(0)}\,\mathrm{d}\eta''\,\mathrm{d}\eta' \to 0, \quad \overline{W}^{(0)} \to 0 \quad (\eta \to \pm\infty), \tag{6.7a}$$

$$\int^\eta \hat{U}_-^{(1)}\,\mathrm{d}\eta' \to 0, \quad \int^\eta \hat{U}_+^{(1)}\,\mathrm{d}\eta' \to 0, \quad \overline{W}^{(1)} \to \mp\frac{\mathrm{i}}{\sin\theta}\overline{V}_\infty \quad (\eta \to \pm\infty). \tag{6.7b}$$

We remark that the constant $\overline{V}_\infty$ that appears in (6.6*a*) and (6.6*b*) and the boundary conditions (6.7*b*) is unknown. However, (6.6*a*)–(6.6*c*) which reflect the $O(1)$ term balance in (3.7)–(3.9), along with the leading-order boundary conditions (6.7*a*), cannot determine $\overline{V}_\infty$ as well as $\hat{U}_-^{(0)}$, $\hat{U}_+^{(0)}$, $\overline{W}^{(0)}$ and c. Rather, it is the combined equation system (6.6) together with the full boundary conditions (6.7) that define a suitable eigenvalue problem for $(\hat{U}_-^{(0)}, \hat{U}_+^{(0)}, \overline{W}^{(0)}, \hat{U}_-^{(1)}, \hat{U}_+^{(1)}, \overline{W}^{(1)})$, with c being the eigenvalue; $\overline{V}_\infty$ is thus found as part of the solution of this problem via satisfying the matching conditions for $\overline{W}^{(1)}$ in (6.7*b*).

6.2. *Normalized eigenvalue problem*

In preparation for solving the eigenvalue problem (6.6)–(6.7), we introduce

$$\left.\begin{aligned} \psi_\pm &= \int^\eta\int^{\eta'}\hat{U}_\pm^{(0)}\,\mathrm{d}\eta''\,\mathrm{d}\eta', \quad \varphi = -\mathrm{i}\tan\theta\int^\eta \overline{W}^{(0)}\,\mathrm{d}\eta', \\ \Psi_\pm &= \frac{1}{\sigma}\int^\eta \hat{U}_\pm^{(1)}\,\mathrm{d}\eta', \quad \Phi = -\mathrm{i}\sigma\tan\theta\,\overline{W}^{(1)}. \end{aligned}\right\} \tag{6.8}$$

In terms of these variables and after the scalings

$$\sigma = \frac{1}{2}\cot\theta\,\tilde{\sigma}, \quad c = \cos\theta\,\tilde{c}, \quad U = \frac{1}{2}\cos\theta\,\tilde{U}, \quad \overline{V}_\infty = \frac{\cot\theta}{\sigma}\,V, \tag{6.9}$$

equations (6.6) and the boundary conditions (6.7) read

$$\tilde{c}\frac{\mathrm{d}^2\psi_-}{\mathrm{d}\eta^2} = -\mathrm{i}\frac{\mathrm{d}\psi_-}{\mathrm{d}\eta} + \frac{\mathrm{i}}{\tilde{\sigma}}\frac{\mathrm{d}\tilde{U}}{\mathrm{d}\eta}V, \tag{6.10a}$$

$$\tilde{c}\frac{\mathrm{d}^2\psi_+}{\mathrm{d}\eta^2} = \mathrm{i}\frac{\mathrm{d}\psi_+}{\mathrm{d}\eta} + \frac{\mathrm{i}}{\tilde{\sigma}}\frac{\mathrm{d}\tilde{U}^*}{\mathrm{d}\eta}V, \tag{6.10b}$$

$$\tilde{c}\frac{\mathrm{d}^2\varphi}{\mathrm{d}\eta^2} = -\frac{\mathrm{d}\tilde{U}^*}{\mathrm{d}\eta}\frac{\mathrm{d}\psi_-}{\mathrm{d}\eta} - \frac{\mathrm{d}\tilde{U}}{\mathrm{d}\eta}\frac{\mathrm{d}\psi_+}{\mathrm{d}\eta}, \tag{6.10c}$$

$$\tilde{c}\frac{\mathrm{d}\Psi_-}{\mathrm{d}\eta} = -\mathrm{i}\Psi_- + \frac{1}{\tilde{\sigma}}\psi_- + \frac{\mathrm{i}}{\tilde{\sigma}}\frac{\mathrm{d}\tilde{U}}{\mathrm{d}\eta}\varphi, \tag{6.10d}$$

$$\tilde{c}\frac{\mathrm{d}\Psi_+}{\mathrm{d}\eta} = \mathrm{i}\Psi_+ - \frac{1}{\tilde{\sigma}}\psi_+ + \frac{\mathrm{i}}{\tilde{\sigma}}\frac{\mathrm{d}\tilde{U}^*}{\mathrm{d}\eta}\varphi, \tag{6.10e}$$

$$\tilde{c}\frac{\mathrm{d}\Phi}{\mathrm{d}\eta} = -\frac{\mathrm{d}\tilde{U}^*}{\mathrm{d}\eta}\left(\Psi_- + \frac{\mathrm{i}}{\tilde{\sigma}}\psi_-\right) - \frac{\mathrm{d}\tilde{U}}{\mathrm{d}\eta}\left(\Psi_+ + \frac{\mathrm{i}}{\tilde{\sigma}}\psi_+\right), \tag{6.10f}$$

with

$$\left.\begin{aligned} &\psi_- \to 0, \quad \psi_+ \to 0, \quad \frac{\mathrm{d}\varphi}{\mathrm{d}\eta} \to 0, \\ &\Psi_- \to 0, \quad \Psi_+ \to 0, \quad \Phi \to \frac{\mp V}{\sin\theta} \quad (\eta \to \pm\infty). \end{aligned}\right\} \tag{6.11}$$

This eigenvalue problem, which replaces (5.4)–(5.5) for $\mu = O(\varepsilon^{3/2})$, was solved numerically by the procedure described earlier (see § 5.1), choosing again (5.6) for the normalized beam profile $\tilde{U}(\eta)$. To compute the constant mean flow V, in particular, Φ was eliminated in favour of V by integrating (6.10*f*) from $\eta = -\infty$ to $\eta = \infty$ and using (6.10*d*), (6.10*e*) and the matching conditions for Φ in (6.11):

$$V = \frac{\mathrm{i}\sin\theta}{2}\int_{-\infty}^{\infty}\left(\frac{\mathrm{d}\tilde{U}^*}{\mathrm{d}\eta}\frac{\mathrm{d}\Psi_-}{\mathrm{d}\eta} - \frac{\mathrm{d}\tilde{U}}{\mathrm{d}\eta}\frac{\mathrm{d}\Psi_+}{\mathrm{d}\eta}\right)\mathrm{d}\eta. \tag{6.12}$$

Since the beam angle θ appears explicitly in (6.12), eigenvalues $\tilde{c}$ now depend on three parameters, θ, $\tilde{\sigma}$ and the beam peak amplitude U_0. Specific results for progressive and standing beams are presented below.

6.3. *Progressive beams*

Computed eigenvalues $\tilde{c} = \tilde{c}_r + \mathrm{i}\tilde{c}_i$ with $\tilde{c}_i < 0$ for progressive beams versus $\tilde{\sigma}$ are plotted in figure 8 for the same values of $U_0 = 0.35$, 0.5 and 0.65 as in figure 3, and $\theta = \pi/6$ and $\pi/3$. (For these parameter values beams are statically stable according to (5.7).) Note that, for given U_0 and θ, as $\tilde{\sigma} \to 0$, $\tilde{c}$ approaches the corresponding asymptotic value of $\tilde{c}$ found earlier as $\tilde{\kappa} \to \infty$ in figure 3. The stability results for $\mu = O(\varepsilon^{3/2})$ presented here are thus smoothly connected with those obtained in § 5.2 for $\mu = O(\varepsilon^2)$.

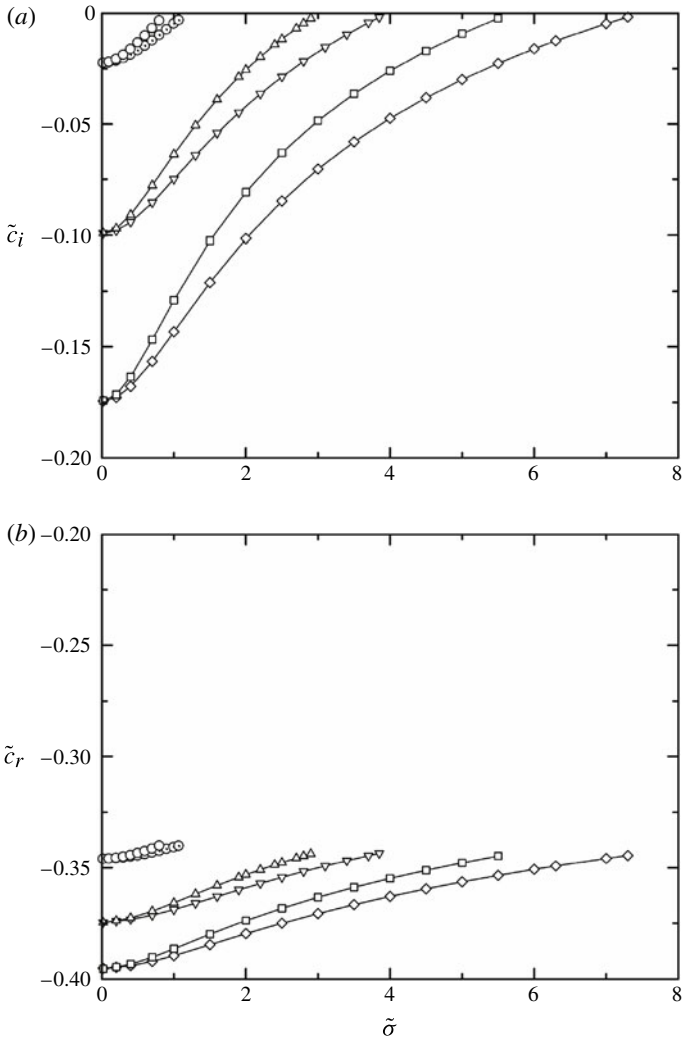

FIGURE 8. Computed unstable eigenvalues $\tilde{c} = \tilde{c}_r + \mathrm{i}\tilde{c}_i$ (with $\tilde{c}_i < 0$) versus $\tilde{\sigma}$ for progressive beams (5.6*a*), with $\theta = \pi/6$ and $U_0 = 0.35$ (○), 0.5 (△) and 0.65 (□), and with $\theta = \pi/3$ and $U_0 = 0.35$ (⊙), 0.5 (▽) and 0.65 (◇); (*a*) $\tilde{c}_i$ versus $\tilde{\sigma}$, (*b*) $\tilde{c}_r$ versus $\tilde{\sigma}$.

Figure 8 shows that modes with negative $\tilde{c}_i$ are possible only for a finite range of $\tilde{\sigma} \geqslant 0$. The associated instability growth rate, $-\tilde{\sigma}\tilde{c}_i$, which is an increasing function of $\tilde{\sigma}$ for small $\tilde{\sigma}$, thus reaches a peak at some finite $\tilde{\sigma}$ and finally falls to zero at a higher $\tilde{\sigma}$; hence, unstable perturbations are always oblique to the beam direction. This result underscores the three-dimensional character of the instability mechanism, and is also consistent with Tabaei & Akylas (2003), who found that purely longitudinal modulations ($\tilde{\sigma} \to \infty$) are stable.

A representative example of an unstable eigenmode is displayed in figure 9. As expected, $\overline{V}_\infty$ and $\overline{W}^{(1)}$ are not localized in η. Rather, by virtue of the boundary conditions (6.7), this inner solution is connected to the outer solution (4.8)

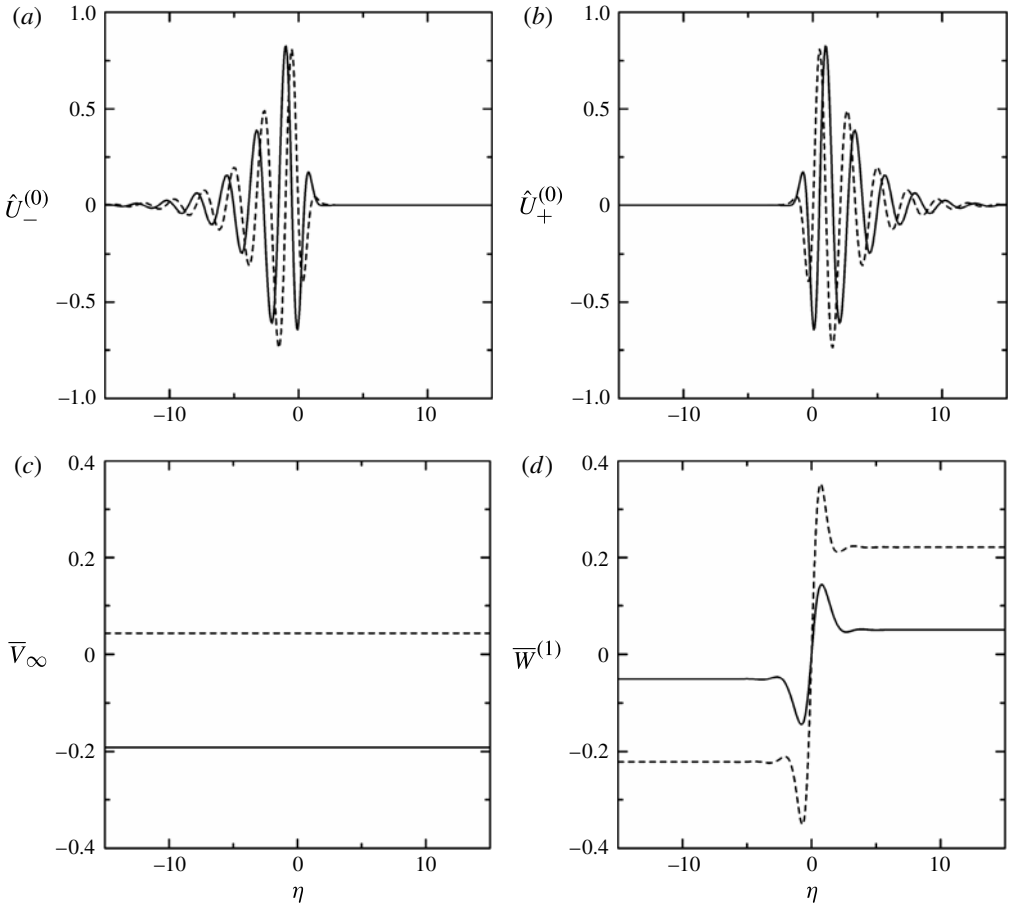

FIGURE 9. Eigenmode with the highest growth rate (at $\tilde{\sigma} = 1.65$) versus η for progressive beam (5.6*a*) with $U_0 = 0.5$ and $\theta = \pi/3$: (*a*) $\hat{U}_-^{(0)}$, (*b*) $\hat{U}_+^{(0)}$, (*c*) $\overline{V}_\infty$, (*d*) $\overline{W}^{(1)}$. The solid line is the real part, and the dashed line is the imaginary part under the normalization $\int_{-\infty}^{\infty} \hat{U}_-^{(0)}(\mathrm{d}\tilde{U}^*/\mathrm{d}\eta)\,\mathrm{d}\eta = 1$.

with $\overline{V}|_{-\infty} = \overline{V}|_{\infty} = \overline{V}_\infty$, which represents an $O(\varepsilon^{3/2})$ single circulating horizontal flow per half transverse wavelength (figure 5*a*).

6.4. *Standing beams*

Computed unstable eigenvalues ($\tilde{c}_i < 0$) for standing beams versus $\tilde{\sigma}$ are plotted in figure 10 for the same values of $U_0 = 0.1$, 0.4 and 0.65 as in figure 6, and $\theta = \pi/6$ and $\pi/3$. (For these parameter values beams satisfy the criterion (5.7) for static stability.) All eigenvalues are pure imaginary, similarly to those shown in figure 6. Moreover, upon comparing these two sets of results, it is seen that, for given U_0 and θ, the limiting values of $\tilde{c}$ as $\tilde{\sigma} \to 0$ here agree with the asymptotic values of $\tilde{c}$ as $\tilde{\kappa} \to \infty$ in the earlier computations (figure 6); hence, matching is achieved. Finally, as in the case of progressive beams (§ 6.3), the instability growth rate, $-\tilde{\sigma}\tilde{c}_i$, after attaining a maximum falls to zero at a finite value of $\tilde{\sigma}$. Therefore, the instability is again three-dimensional.

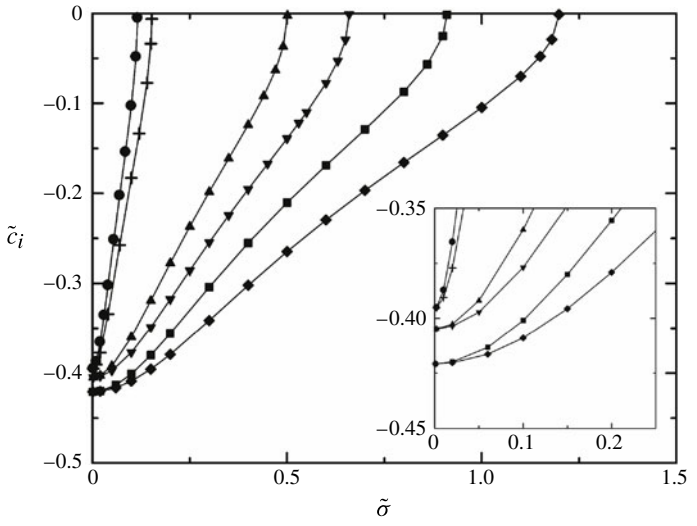

FIGURE 10. Computed unstable eigenvalues $\tilde{c} = \mathrm{i}\tilde{c}_i$ versus $\tilde{\sigma}$ for standing beams (5.6*b*), with $\theta = \pi/6$ and $U_0 = 0.1$ (●), 0.4 (▲) and 0.65 (■), and with $\theta = \pi/3$ and $U_0 = 0.1$ (+), 0.4 (▼) and 0.65 (♦). The inset shows a close-up of the plot near $\tilde{\sigma} = 0$.

7. Discussion

The preceding analysis has revealed that beam modulations that vary both in the along-beam and the horizontal transverse directions behave very differently from purely longitudinal beam modulations considered in Tabaei & Akylas (2003). Such oblique modulations enable the coupling of a uniform beam to three-dimensional perturbations that involve a time-harmonic component, with the beam frequency, and a mean flow; as a result of this resonant first-harmonic–mean-flow interaction, energy can be extracted from a uniform beam, causing instability.

An interesting feature of this instability mechanism is that the mean-flow component of unstable perturbations extends far from the vicinity of the underlying wave beam. Theoretically, this necessitates the use of matched asymptotic expansions for deriving the appropriate stability eigenvalue problem for the complex perturbation speed, $c = c_r + \mathrm{i}c_i$. As it turns out, the proper asymptotic treatment hinges on whether the beam steepness is assumed to be infinitesimally small or finite, and the stability results are fundamentally distinct in these two instances. Specifically, in the small-steepness limit, progressive beams are entirely stable, whereas purely standing beams are always unstable. On the other hand, in the finite-steepness regime, progressive beams become unstable above a certain threshold steepness, while purely standing beams continue to be unstable irrespective of their steepness. In all cases, however, instability arises solely due to oblique modulations.

Apart from the beam steepness, another parameter that affects the instability of finite-steepness beams is θ, the beam angle to the horizontal, as indicated by the scalings (6.9). To bring out this dependence, we plot in figure 11(*a*) the computed maximum growth rate $-\sigma c_i|_{max}$ versus θ in the range $3^\circ \leqslant \theta \leqslant 12^\circ$, for finite-steepness progressive beams with normalized profile (5.6*a*) and amplitudes $U_0 = 0.35$, 0.43 and 0.5. (These beams are all statically stable according to the criterion (5.7).) It is seen that the instability becomes significantly stronger as θ is decreased, particularly below 10° or so, which, interestingly, is the opposite trend from that exhibited by

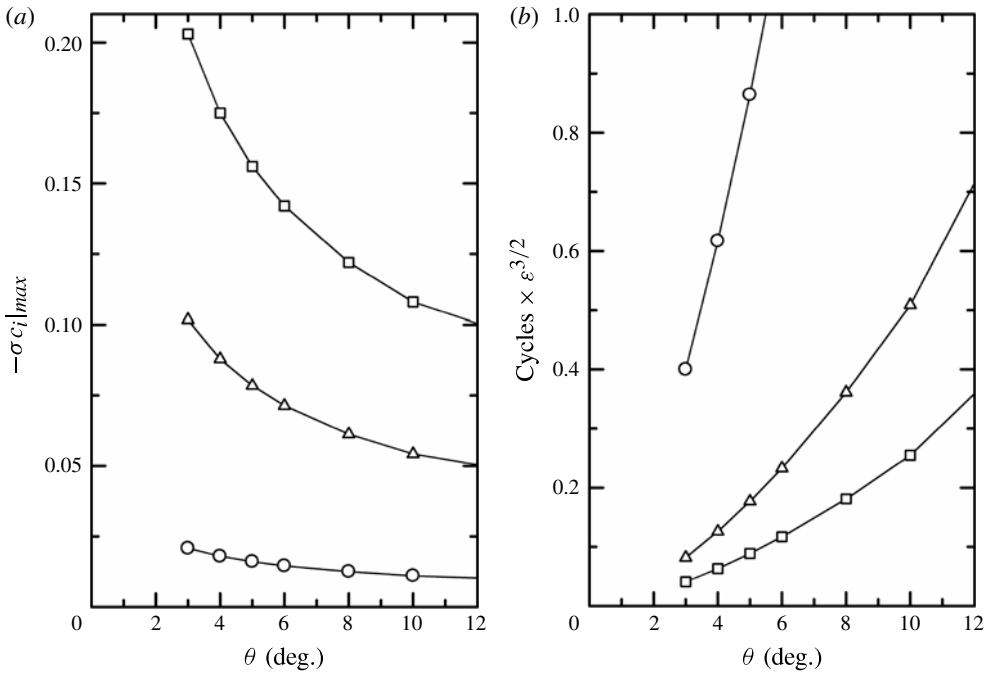

FIGURE 11. Dependence on beam angle to the horizontal θ, of modulational instability of finite-steepness progressive beams with profile (5.6*a*), with amplitude $U_0 = 0.35$ (◯), 0.43 (△) and 0.5 (□). (*a*) Computed maximum growth rate $-\sigma\, c_i|_{max}$. (*b*) Cycles $\times \varepsilon^{3/2}$, in terms of beam period, it would take the most unstable disturbance to amplify by a factor of e.

parametric subharmonic instability of periodic wavetrains (Lombard & Riley 1996). This suggests that three-dimensional modulational instability should be relevant to steep tidally generated wave beams, which are of the progressive type and propagate at small θ, typically in the 3–5° range. To emphasize this point further, figure 11(*b*) shows the number of cycles, in terms of beam period, it would take the most unstable disturbance to amplify by a factor of e, for the same beams and θ as in figure 11(*a*). Clearly, for θ in the range relevant to tidally generated beams, the instability is expected to grow appreciably within a tidal period.

While our asymptotic analysis applies to beams with general locally confined profile, here specific results were reported only for the progressive- and standing-beam profiles (5.6) with $A(l) = -l^2 \mathrm{e}^{-l^2/8}/\sqrt{8\pi}$. However, we did carry out computations for various other localized profiles and the results turned out to be qualitatively the same. For example, substituting $A(l) = -l^3 \mathrm{csch}(\pi l/2)$ in (5.6*a*), the critical U_0 above which progressive beams become unstable is now ∼0.37 compared to 0.3 for the earlier choice of $A(l)$. In view of (2.3*a*) and (5.3), given a progressive beam profile, the dimensionless critical amplitude U_0 translates into a peak vertical displacement of $O(U_0 L \cos\theta)$, which provides a dimensional threshold for instability in terms of the (dimensional) characteristic beam width L and propagation angle θ.

In assessing the three-dimensional instability mechanism discussed here, it should be kept in mind that our results are based on an asymptotic approach, valid for long-wavelength perturbations relative to the beam thickness ($\varepsilon,\ \mu \ll 1$). Accordingly, the predicted maximum instability growth rates are small, $-\sigma\, c_i|_{max}\varepsilon^{3/2} \ll 1$, but increasing

as ε is increased. Of course, this trend strictly holds for $\varepsilon \ll 1$, and understanding the instability of wave beams to oblique perturbations with $\varepsilon = O(1)$ would require a fully numerical stability analysis. Also, as remarked earlier, our theory becomes singular when $\theta = 0$, as the beam frequency is zero in this limit.

Finally, the present study has ignored background rotation, which does come into play in a geophysical setting, due to the Earth's rotation. In regard to tidally generated internal wave beams, however, rotation would mainly cause the beam angle θ to slightly decrease, and modulational instability is unlikely to be affected in a significant way by this modification. On the other hand, the Earth's rotation plays a crucial role in the parametric subharmonic instability of tidal beams with frequency close to twice the inertial frequency (Gerkema, Staquet & Bouruet-Aubertot 2006; Young, Tsang & Balmforth 2008), but this instability mechanism is quite distinct from the one discussed here.

Acknowledgements

This work was supported in part by the US National Science Foundation under grant DMS-1107335 and by Kobe Technical Club (KTC).

Appendix. Small-steepness beams

For small-steepness beams ($|U| \ll 1$), it is necessary to rescale (3.7)–(3.9) in order to obtain the appropriate eigenvalue problem for determining c. To this end, we put

$$U(\eta) = \delta\, U_S(\eta), \tag{A 1}$$

where $|U_S| = O(1)$ and δ is a small parameter ($0 < \delta \ll 1$) that will be related to ε. Here, μ and ε are assumed to satisfy (3.1) with $\kappa = O(1)$. From (3.8), then, $\overline{W} = O(\delta)$, and $\overline{V}$ must be constant to leading order according to (3.9). Turning next to (3.7), since the beam profile $U = O(\delta)$, for the interaction terms coupling $\hat{U}_+$ and $\hat{U}_-$ with U to come into play – this is essential to the instability mechanism – it is necessary that $\overline{V} = O(1/\delta)$. Hence, $\overline{V}$ and $\overline{U}$ (according to (3.10)) are increased by a factor of $1/\delta$, whereas $\overline{W}$ is decreased by a factor of δ. Now, this mean flow must be matched to the outer solution (4.8); for this to be possible, in view of (3.1) and (3.2), it is necessary that $\varepsilon\delta \sim \varepsilon^2/\delta$, suggesting that

$$\delta = \varepsilon^{1/2}. \tag{A 2}$$

Based on the above qualitative arguments, the mean flow is rescaled as

$$\overline{U} \to \varepsilon^{-1/2} \cot\theta\, \overline{V}_\infty, \quad \overline{V} \to \varepsilon^{-1/2}\overline{V}_\infty, \quad \overline{W} \to \kappa\varepsilon^{1/2}\overline{W}, \tag{A 3}$$

where $\overline{V}_\infty$ is constant, and upon substituting (A 1)–(A 3) into (3.7) and (3.8), we find

$$c\hat{U}_- = \cos\theta \left(-\mathrm{i}\frac{\mathrm{d}}{\mathrm{d}\eta} + \frac{\cot\theta}{2\kappa}\right) \int^\eta \int^{\eta'} \hat{U}_-\, \mathrm{d}\eta''\, \mathrm{d}\eta' + \mathrm{i}\frac{\mathrm{d}U_S}{\mathrm{d}\eta}\overline{V}_\infty, \tag{A 4a}$$

$$c\hat{U}_+ = \cos\theta \left(\mathrm{i}\frac{\mathrm{d}}{\mathrm{d}\eta} - \frac{\cot\theta}{2\kappa}\right) \int^\eta \int^{\eta'} \hat{U}_+\, \mathrm{d}\eta''\, \mathrm{d}\eta' + \mathrm{i}\frac{\mathrm{d}U_S^*}{\mathrm{d}\eta}\overline{V}_\infty, \tag{A 4b}$$

$$\begin{aligned} c\frac{\mathrm{d}\overline{W}}{\mathrm{d}\eta} = \frac{2\cot\theta}{\kappa} \Bigg\{ &\frac{\mathrm{d}U_S^*}{\mathrm{d}\eta} \left(-\mathrm{i}\frac{\mathrm{d}}{\mathrm{d}\eta} + \frac{\cot\theta}{2\kappa}\right) \int^\eta \int^{\eta'} \hat{U}_-\, \mathrm{d}\eta''\, \mathrm{d}\eta' \\ &+ \frac{\mathrm{d}U_S}{\mathrm{d}\eta} \left(-\mathrm{i}\frac{\mathrm{d}}{\mathrm{d}\eta} + \frac{\cot\theta}{2\kappa}\right) \int^\eta \int^{\eta'} \hat{U}_+\, \mathrm{d}\eta''\, \mathrm{d}\eta' \Bigg\}. \end{aligned} \tag{A 4c}$$

In addition, from (4.1) and matching of the mean-flow perturbation with the outer solution (4.7)–(4.9) (which is upgraded here by $O(\varepsilon^{-1/2})$), the following boundary conditions are imposed:

$$\int^{\eta}\int^{\eta'}\hat{U}_-\,\mathrm{d}\eta''\,\mathrm{d}\eta'\to 0,\quad \int^{\eta}\int^{\eta'}\hat{U}_+\,\mathrm{d}\eta''\,\mathrm{d}\eta'\to 0,\quad \overline{W}\to\mp\frac{\mathrm{i}\overline{V}_\infty}{\sin\theta}\quad(\eta\to\pm\infty)\text{(A 5)}$$

Equations (A 4) subject to the boundary conditions (A 5) constitute the desired eigenvalue problem for determining c in the small-steepness limit. Again, as in (6.10) and (6.11), the constant mean flow $\overline{V}_\infty$ is an unknown, to be found as part of the solution of this problem. Letting

$$\varphi=-\frac{\mathrm{i}}{2}\sqrt{\sin\theta}\,\overline{W},\quad \overline{V}_\infty=2\sqrt{\sin\theta}\,V,\quad U_S=\frac{\cos\theta}{2\sqrt{\sin\theta}}\,\tilde{U}_S,\tag{A 6}$$

and using the same notation as in (5.1) and (5.3) for $\psi_\pm$, $\tilde{\kappa}$ and $\tilde{c}$, we obtain a normalized version of the eigenvalue problem, with θ completely scaled out, for (ψ_-,ψ_+,φ):

$$\tilde{c}\frac{\mathrm{d}^2\psi_-}{\mathrm{d}\eta^2}=-\mathrm{i}\frac{\mathrm{d}\psi_-}{\mathrm{d}\eta}+\frac{\psi_-}{\tilde{\kappa}}+\mathrm{i}\frac{\mathrm{d}\tilde{U}_S}{\mathrm{d}\eta}V,\tag{A 7a}$$

$$\tilde{c}\frac{\mathrm{d}^2\psi_+}{\mathrm{d}\eta^2}=\mathrm{i}\frac{\mathrm{d}\psi_+}{\mathrm{d}\eta}-\frac{\psi_+}{\tilde{\kappa}}+\mathrm{i}\frac{\mathrm{d}\tilde{U}_S^*}{\mathrm{d}\eta}V,\tag{A 7b}$$

$$\tilde{c}\frac{\mathrm{d}\varphi}{\mathrm{d}\eta}=-\frac{1}{\tilde{\kappa}}\left\{\frac{\mathrm{d}\tilde{U}_S^*}{\mathrm{d}\eta}\left(\frac{\mathrm{d}\psi_-}{\mathrm{d}\eta}+\frac{\mathrm{i}}{\tilde{\kappa}}\psi_-\right)+\frac{\mathrm{d}\tilde{U}_S}{\mathrm{d}\eta}\left(\frac{\mathrm{d}\psi_+}{\mathrm{d}\eta}+\frac{\mathrm{i}}{\tilde{\kappa}}\psi_+\right)\right\},\tag{A 7c}$$

subject to

$$\psi_-\to 0,\quad \psi_+\to 0,\quad \varphi\to\mp V\quad(\eta\to\pm\infty).\tag{A 8}$$

In solving the above problem, it is convenient to eliminate φ in favour of V, by integrating (A 7*c*) and using (A 7*a*), (A 7*b*) and the matching condition for φ in (A 8), as was done in (6.12).

Taking into account the various rescalings of U in (A 1), (A 2), (A 6) and (5.3), the beam steepness parameter U_0 in (5.6) is related to its small-steepness counterpart U_{S0} via

$$U_0=\frac{\varepsilon^{1/2}}{\sqrt{\sin\theta}}\,U_{S0}.\tag{A 9}$$

REFERENCES

ALEXANDER, M. J., HOLTON, J. R. & DURRAN, D. R. 1995 The gravity wave response above deep convection in a squall line simulation. *J. Atmos. Sci.* **52**, 2212–2226.

BELL, T. H. 1975 Lee waves in stratified flows with simple harmonic time dependence. *J. Fluid Mech.* **67**, 705–722.

BORDES, G., VENAILLE, A., JOUBAUD, S., ODIER, P. & DAUXOIS, T. 2012 Experimental observation of a strong mean flow induced by internal gravity waves. *Phys. Fluids* **24**, 086602.

CLARK, H. A. & SUTHERLAND, B. R. 2010 Generation, propagation, and breaking of an internal wave beam. *Phys. Fluids* **22**, 076601.

COLE, S. T., RUDNICK, D. L., HODGES, B. A. & MARTIN, J. P. 2009 Observations of tidal internal wave beams at Kauai Channel, Hawaii. *J. Phys. Oceanogr.* **39**, 421–436.

DEWAN, E. M., PICARD, R. H., O'NEIL, R. R., GARDINER, H. A. & GIBSON, J. 1998 MSX satellite observations of thunderstorm-generated gravity waves in mid-wave infrared images of the upper stratosphere. *Geophys. Res. Lett.* **25**, 939–942.

FOVELL, R., DURRAN, D. & HOLTON, J. R. 1992 Numerical simulations of convectively generated stratospheric gravity waves. *J. Atmos. Sci.* **49**, 1427–1442.

GERKEMA, T., STAQUET, C. & BOURUET-AUBERTOT, P. 2006 Decay of semi-diurnal internal-tide beams due to subharmonic resonance. *Geophys. Res. Lett.* **33**, L08604.

GOSTIAUX, L. & DAUXOIS, T. 2007 Laboratory experiments on the generation of internal tidal beams over steep slopes. *Phys. Fluids* **19**, 028102.

JOHNSTON, T. M. S., RUDNICK, D. L., CARTER, G. S., TODD, R. E. & COLE, S. T. 2011 Internal tidal beams and mixing near Monterey Bay. *J. Geophys. Res.* **116**, C03017.

KHATIWALA, S. 2003 Generation of internal tides in an ocean of finite depth: analytical and numerical calculations. *Deep-Sea Res.* **50**, 3–21.

KING, B., ZHANG, H. P. & SWINNEY, H. L. 2009 Tidal flow over three-dimensional topography in a stratified fluid. *Phys. Fluids* **21**, 116601.

KOUDELLA, C. R. & STAQUET, C. 2006 Instability mechanisms of a two-dimensional progressive internal gravity wave. *J. Fluid Mech.* **548**, 165–196.

KUMAR, K. K. 2007 VHF radar investigations on the role of mechanical oscillator effect in exciting convectively generated gravity waves. *Geophys. Res. Lett.* **34**, L01803.

LAMB, K. G. 2004 Nonlinear interaction among internal wave beams generated by tidal flow over supercritical topography. *Geophys. Res. Lett.* **31**, L09313.

LIEN, R.-C. & GREGG, M. C. 2001 Observations of turbulence in a tidal beam and across a coastal ridge. *J. Geophys. Res.* **106**, 4575–4591.

LIGHTHILL, M. J. 1978 *Waves in Fluids*. Cambridge University Press.

LOMBARD, P. N. & RILEY, J. J. 1996 Instability and breakdown of internal gravity waves. Part 1. Linear stability analysis. *Phys. Fluids* **8**, 3271–3287.

MCEWAN, A. D. 1973 Interactions between internal gravity waves and their traumatic effect on a continuous stratification. *Boundary-Layer Meteorol.* **5**, 159–175.

MOWBRAY, D. E. & RARITY, B. S. H. 1967 A theoretical and experimental investigation of the phase configuration of internal waves of small amplitude in a density stratified fluid. *J. Fluid Mech.* **28**, 1–16.

PEACOCK, T., ECHEVERRI, P. & BALMFORTH, N. J. 2008 An experimental investigation of internal tide generation by two-dimensional topography. *J. Phys. Oceanogr.* **38**, 235–242.

TABAEI, A. & AKYLAS, T. R. 2003 Nonlinear internal gravity wave beams. *J. Fluid Mech.* **482**, 141–161.

TABAEI, A., AKYLAS, T. R. & LAMB, K. G. 2005 Nonlinear effects in reflecting and colliding internal wave beams. *J. Fluid Mech.* **526**, 217–243.

YOUNG, W. R., TSANG, Y.-K. & BALMFORTH, N. J. 2008 Near-inertial parametric subharmonic instability. *J. Fluid Mech.* **607**, 25–49.

ZHANG, H. P., KING, B. & SWINNEY, H. L. 2007 Experimental study of internal gravity waves generated by supercritical topography. *Phys. Fluids* **19**, 096602.